Title

Energy reconstruction of an n-type segmented inverted coaxial point-contact HPGe detector

Authors

Salathe, M
Cooper, RJ
Crawford, HL
et al.

Publication Date

2017-10-01

DOI

10.1016/j.nima.2017.06.036

Peer reviewed

Energy reconstruction of an n-type segmented inverted coaxial point-contact HPGe detector

M. Salathe[a,*], R. J. Cooper[a], H. L. Crawford[a], D. C. Radford[b], J. M. Allmond[b], C. M. Campbell[a], R. M. Clark[a], M. Cromaz[a], P. Fallon[a], P. A. Hausladen[c], M. D. Jones[a], A. O. Macchiavelli[a], J. P. Wright[d]

[a] *Nuclear Science Division, Lawrence Berkeley National Laboratory, 1 Cyclotron Rd, Berkeley, CA 94720, USA*
[b] *Physics Division, Oak Ridge National Laboratory, 1 Bethel Valley Rd, Oak Ridge, TN 37831, USA*
[c] *Nuclear Security and Isotope Technology Division, Oak Ridge National Laboratory, 1 Bethel Valley Rd, Oak Ridge, TN 37831, USA*
[d] *Oliver Lodge Laboratory, University of Liverpool, Liverpool, L69 7ZE, United Kingdom*

Abstract

We have characterized, for the first time, an n-type segmented inverted coaxial point-contact detector. This novel detector technology relies on a large variation in drift time of the majority charge carriers, as well as image and net charges observed on the segments, to achieve a potential γ-ray interaction position resolution of better than 1 mm. However, the intrinsic energy resolution in this detector is poor (more than 20 keV at 1332 keV) because of charge (electron) trapping effects. We propose an algorithm that enables restoration of the resolution to a value of 3.44±0.03 keV at 1332 keV for events with a single interaction. The algorithm is based on a measurement of the azimuthal angle and the electron drift time of a given event; the energy of the event is corrected as a function of these two values.

Keywords: High purity germanium detectors, γ-ray tracking, γ-ray imaging, Electron trapping correction

1. Introduction

The Inverted Coaxial Point-Contact (ICPC) detector, a novel large-volume High Purity Germanium (HPGe) technology, combines a small circular electrode, or point contact, with the typical shape and volume of a coaxial detector [1]. The small dimension of the point contact serves to reduce capacitance and therefore series noise. Low electric fields in most of the detector volume and generally long drift paths increase the charge collection time compared to conventional detectors. The farther away from the point contact an interaction occurs, the longer it takes the majority charge carriers to drift to the point contact. Furthermore, the pronounced weighting field around the electrode leads to a characteristic pulse shape. This pulse shape together with the variation in drift time can be used to determine the number of interactions in the detector [2]. The addition of a bore hole in the detector bypasses the volume limitations of cylindrical point-contact detectors, which if too large cannot be fully depleted at a reasonable bias voltage (a few thousand volts).

The outer surface and bore-hole contacts of the ICPC detector can be subdivided into segments. These segments not only collect the minority charge carriers, but are also sensitive to image charges induced as the majority charge carriers drift towards the point contact. The signals observed on the segments, together with the signal measured on the point contact, can be used to reconstruct the exact location of the charge deposition within the detection volume with sub-segment precision. A prior analytic study of these detectors predicted sub-millimeter three-dimensional position resolution [1], on average a factor of four to five better than segmented coaxial detectors [3].

However, for an n-type ICPC detector, where electrons are the majority charge carriers, the intrinsic energy resolution is poor as compared to p-type detectors[1]. Crystal impurities and defects result in a fraction of the drifting electrons being trapped and thus not contributing to the signal observed at the read-out electrode. Trapping in conventional coaxial detectors, where electrons are collected over a short distance in high electric fields, is typically small. In the ICPC detector, the time electrons drift before being collected at the point contact can be significant and depends on the location of the γ-ray interaction. This affects the amount of electron trapping and thus the measured energy. A typical measurement consists of γ rays interacting at many different locations and thus the overall energy resolution is deteriorated.

In this work, we will demonstrate that trapping induced energy deficits can be compensated for by extract-

*Corresponding author
Email addresses: msalathe@lbl.gov (M. Salathe), rjcooper@lbl.gov (R. J. Cooper), hlcrawford@lbl.gov (H. L. Crawford), radforddc@ornl.gov (D. C. Radford)

[1] It is possible to produce detectors so that holes are the majority charge carriers (p-type). These detectors have a very good intrinsic energy resolution (we have measured 1.8 keV FWHM at 1332 keV for a detector of similar geometry) but are more susceptible to radiation damage.

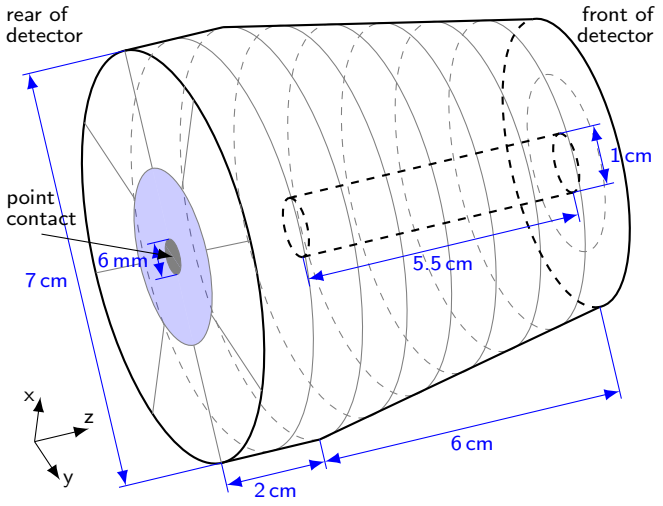

Figure 1: A sketch of the segmented inverted coaxial point-contact detector. The gray lines show the segmentation boundaries. The gray filled area is the point contact, and the blue filled area is a passivated layer.

ing position information from the segment signals and correcting the energy according to the amount of trapping expected for the corresponding electron trajectory. Such an approach has been considered before [4, 5, 6], mostly to correct the effect of hole trapping and not on the scale presented here. The energy correction is based on a reconstruction of the azimuthal angle of γ-ray interactions and the drift time of the electrons. In Sec. 2 the methods used to measure these quantities will be presented. In Sec. 3 we discuss first results from an n-type segmented ICPC detector and show that the proposed method can significantly improve the energy resolution.

2. Methods

In this section, we describe the detector, the measurement setup and simulations used for the characterization of the detector, as well as the methodology used to correct the energy resolution.

2.1. Prototype detector and measurement setup

A schematic of the segmented ICPC detector is shown in Fig. 1. The rear surface around the point contact is subdivided into eight azimuthal segments, while the length of the detector is divided into 8 circular segments and the front face around the bore hole is split into two circular segments. The electrical contact inside the bore hole is itself an additional segment. The detector thus consists of 20 individual read-out channels – 19 for the segments and one for the point contact. The prototype detector was built by Canberra Lingolsheim [7], is produced from n-type material and was operated with 5000 V bias voltage at the point contact. The remaining segments are grounded.

The manufacturer measured the impurity profile of the crystal, which starts at $0.8 \times 10^{10}\,\mathrm{cm}^{-3}$ at the tapered (front) face and reaches $1.6\times10^{10}\,\mathrm{cm}^{-3}$ at the point-contact (rear) face. The exact profile is not known, but is assumed to be linear.

In the present work, the signals observed on the 20 segments were digitized at a sampling rate of 100 MHz using GRETINA digitizers [3]. The digitized signals were shaped with a trapezoidal filter with an integration time of 6 µs and a 2 µs flat top. The pulse height (energy) is measured and stored for all 20 segments. Furthermore, the pulse waveform in a 6 µs window centered on the rising edge was stored to disk for further analysis (i.e. azimuthal reconstruction) for all segments.

The detector was characterized using collimated and uncollimated radioactive sources (^{241}Am, ^{137}Cs and ^{60}Co). Collimated sources were positioned, using an automated scanning table, to irradiate specific (x,y) locations along the endcap of the detector cryostat. The ^{241}Am source emits γ rays at 59.5 keV which are absorbed close to the surface of the germanium. This source was used with a 2 mm collimator to cover a fine grid (2 mm spacing) of measurements across the surface of the detector. The ^{137}Cs source radiates γ rays of 662 keV energy that penetrate farther into the germanium. Thus, this source was used for collimated (1 mm) beam measurements to probe the crystal beyond its surface. The two transitions of ^{60}Co at 1173 keV and 1332 keV were used without a collimator to study events more evenly distributed within the detector volume.

The FWHM resolution of the rear, side and front segments is between 1.8 and 3.0 keV at 1332 keV (uncollimated ^{60}Co). The core segment has a resolution of 12 keV, which is attributed to a poor electrical connection. However, these segments often see only a fraction of an events total energy. To measure the total deposited energy the respective contributions have to be added, which deteriorates the sum energy considerably. Thus, it is necessary to have an independent method to extract the total event energy, which is given by the point contact signal.

2.2. Monte Carlo simulation

The measurement setup has been modeled in Geant4 [8] (including source characteristics and collimator geometry) to simulate γ-ray-interaction patterns within the detector for the given measurement configurations. Based on these simulated interaction locations, the expected signals from the electrodes were calculated using the code Siggen [9]. The code takes into account electric fields, impurity concentrations and the orientation of the crystal axes in order to calculate the charge trajectories and the induced signals on the electrodes. The calculation does not consider the internal distribution of a given charge carrier cloud, instead reduces them to a single point-like structure. The simulated signals can then be processed in a similar manner to the measured signals, and be directly compared to the real data to cross check our understanding of the detector. The comparison between data and simulation will be further discussed in subsequent sections.

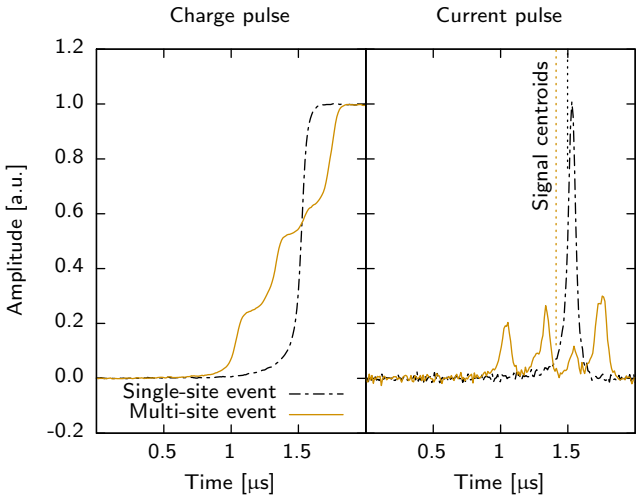

Figure 2: The charge and current pulses of a typical single-site event and an event with multiple interactions. The maximal amplitude in the normalized charge pulse (left) is different for the two topologies. The location of the current signal's centroid, that is used to measure the drift time, is shown as vertical lines in the right plot.

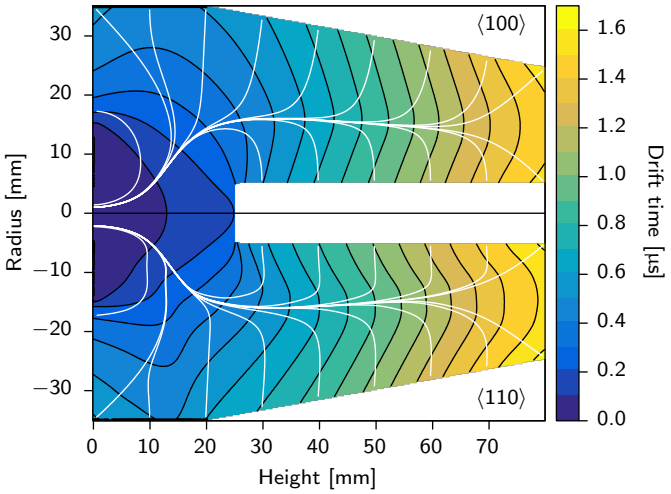

Figure 3: A map of drift-time values found in the detector. The lower and upper halves represent the situation aligned with two distinct crystal axis (at azimuthal angles 45° apart). The z-axis is always aligned with one of the ⟨100⟩ axis. Overlayed are some typical electron drift paths with interactions close to the surface. Electron drift from the interaction location towards the point contact located at (0,0).

2.3. Event topology and drift time

Above a few hundred keV, γ rays usually Compton scatter multiple times and deposit only a fraction of their total energy in each interaction. The full γ-ray energy is thus distributed over multiple interaction sites spread out over the detector volume. The pulse shape that is read-out at the point contact for multi-site events is a superposition of the signals associated with the individual interactions and thus differs from events with a single interaction (see Fig. 2). A simple method to classify these two event topologies is to divide the maximum amplitude (A) of the current signal (derivative of the measured point-contact signal) by the total energy (E), called the A/E value [10]. A low A/E value signifies that an event is more likely multi-site, while a high A/E value indicates that an event is more likely single-site. Disentangling contributions to a signal originating from a multi-site event is complex and is not the focus of the present work. Events were selected to be single-site by defining a lower A/E cut at a distance roughly twice the FWHM value from the single-site event peak centroid. Roughly 13% of all events pass this cut at 1332 keV, 19% at 662keV. Moreover, simulations show that roughly half of these events are composed of multi-site events with interactions separated by less than 20ns in drift time.

Events can also be categorized by the electron drift time. The drift time is the difference between the time when the electrons are created in a γ-ray interaction and the time when they arrive at the point contact. In our measurement, the time of creation is approximated by the time when the segment signal with the highest energy deposition reaches 2% of the full pulse height. The time of collection corresponds to the centroid of the current signal measured on the point contact. For single-site events the pulse shape measured on the point contact is such that the centroid is found at a constant position with respect to the rising edge. The pulse shape of different multi-site events varies widely, however, this definition of the drift time produces consistent results for these events too.

2.4. Charge trapping and recombination

We will not discuss the details of charge trapping and recombination in HPGe detectors – a detailed description of these effects can be found in Ref. [11]. For our purposes, it is simply assumed that upon interaction with a trapping site, electrons are either removed through recombination with a hole, or trapped for a time that exceeds the typical charge collection time (a few microseconds). These charge carriers then do not contribute to the observed signal at the point contact and thus the pulse height (energy) is reduced. Hole trapping and recombination effects are neglected. Furthermore, while charge trapping and/or recombination is believed to be a stochastic process, on average, any charge cloud passing a certain region should experience the same fractional charge loss in that region. Second order effects caused by the actual distribution of charge carriers are neglected.

As a result of the electrode layout of the ICPC design, the trajectories of the majority carriers are of variable length and thus the amount of charge trapping fluctuates. Moreover, trapping centers are inhomogeneously distributed throughout the detector, which further increases fluctuations in the amount of charge lost for different event drift trajectories. However, the electrode design forces the electrons onto largely common paths, located in a central region of the detector between the outside surface and the

inner bore hole. This is illustrated in Fig. 3, which shows the electron trajectories for events evenly distributed over the surface of the detector. As a result, all trajectories following this common path lose, on average, the same fraction of charge carriers in this region. To first order, it is sufficient to correct for this average amount of charge lost on the common path, which reduces the complexity of the problem considerably.

2.5. Azimuth reconstruction

The azimuthal angle of an interaction is extracted based on the net or transient signals observed on the eight azimuthal segments at the rear surface of the detector (see Fig. 1). The algorithm to find the azimuth is as follow:

1. Experimental signals are grouped according to the event drift time and azimuthal angle. All signals in an individual group are averaged to produce a set of segment signals (experimental basis) corresponding to energy depositions with that angle and drift time.
2. The experimental basis signals are compared via a least squares fit to the individual measured signals and a figure of merit is calculated (χ^2).
3. The angle corresponding to the best matching basis (lowest χ^2, including some interpolation between nearest basis points) is selected as the azimuth.

An experimental basis $B(\alpha_\mathrm{i}, t_\mathrm{j})$ was created from collimated ^{137}Cs measurements taken at a detector radius of 24 mm, with 2.5° spacing between measurements. The angle α_i is thus given by the location of the collimator during the measurement. Only events passing the A/E cut that fall within the 662 keV peak and did not induce a net signal into the individual segment were considered. The drift-time range of each measurement (t_j) was divided into 100 ns-wide drift-time regions, each region making up one basis point. An experimental basis signal is constructed by finding the average signal of all events in a given region. In the averaging procedure, the individual signals are time-aligned by the maximum of the point-contact current signals. The basis and the actual signal were compressed to 25 MHz by averaging 4 samples and reduced to a 2 µs region to speed up data processing.

To match the signal shape of the individual events as closely as possible, the two nearest available basis signals (located at drift time t_n and $t_{\mathrm{n}-1}$) for a given event are weighted according to the event's drift time, t, as follows:

$$B(\alpha_\mathrm{i}, t) = B(\alpha_\mathrm{i}, t_\mathrm{n}) \frac{t - t_{\mathrm{n}-1}}{t_\mathrm{n} - t_{\mathrm{n}-1}} + B(\alpha_\mathrm{i}, t_{\mathrm{n}-1}) \frac{t_\mathrm{n} - t}{t_\mathrm{n} - t_{\mathrm{n}-1}} \quad (1)$$

The A/E cut allows for a substantial amount of events with multiple interactions to be included in the basis signal construction. Furthermore, events that make up a single basis point are distributed over a large initial region. Nevertheless, these effects only affect the average pulse shape marginally. Interactions that happen far away from the collimator location, as well as strongly scattered multi-site events occur uniformly around the basis location. Together with the symmetric arrangement of the eight azimuthal segments, the impact of these events is strongly suppressed.

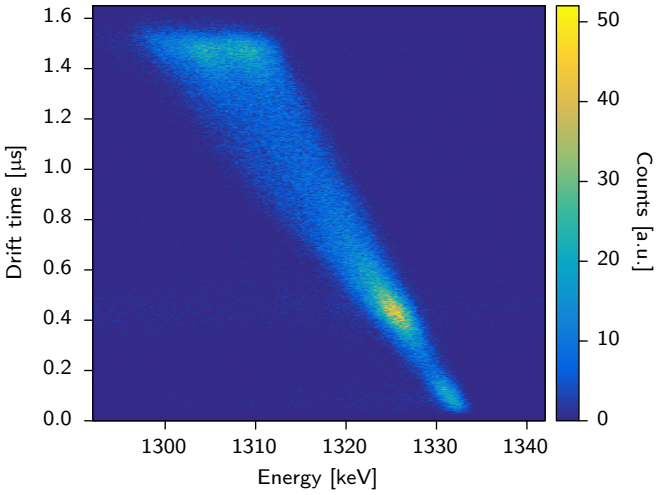

Figure 4: Drift-time dependence of single-site events around the 1332 keV peak of a ^{60}Co measurement. Due to increased trapping the peak is reconstructed at a reduced energy at long drift times.

Based on the drift-time interpolated basis and the actual signal S it is then possible to calculate a figure of merit:

$$\chi^2 = \sum_\mathrm{k} \sum_\mathrm{l} \left(B_\mathrm{kl}(\alpha_\mathrm{i}, t) - S_\mathrm{kl} \right)^2 . \quad (2)$$

Here, the index k corresponds to the segment number and the index l refers to the time sample within the signal. In the calculation of the figure of merit, the signal and the basis are again time-aligned according to the position of the maximum in the point-contact current signal. The basis corresponding to the lowest value of χ^2 indicates at which of the angles α_i the event most likely originated from. An angular value over the continuous range of 0° to 360° is determined between the minimum-figure-of-merit basis, $B(\alpha_\mathrm{m}, t)$, and its nearest angular neighbor, $B(\alpha_\mathrm{n}, t)$, by finding the value a that minimizes

$$\sum_\mathrm{k} \sum_\mathrm{l} \left(a \cdot B_\mathrm{kl}(\alpha_\mathrm{m}, t) + (1 - a) \cdot B_\mathrm{kl}(\alpha_\mathrm{n}, t) - S_\mathrm{kl} \right)^2 . \quad (3)$$

The results, including the precision of the method and its shortcomings are discussed in Sec. 3.2.

2.6. Energy correction

Intuition suggests that the amount of charge trapping should increase in proportion to the time that charges drift through the detector volume. Fig. 4 shows this to be true – the amount of charge trapping, observed as a reduced net energy for long drift-time events, increases almost linearly with drift time. This linear effect is thus easily removed by multiplying the energy with a correction factor that is

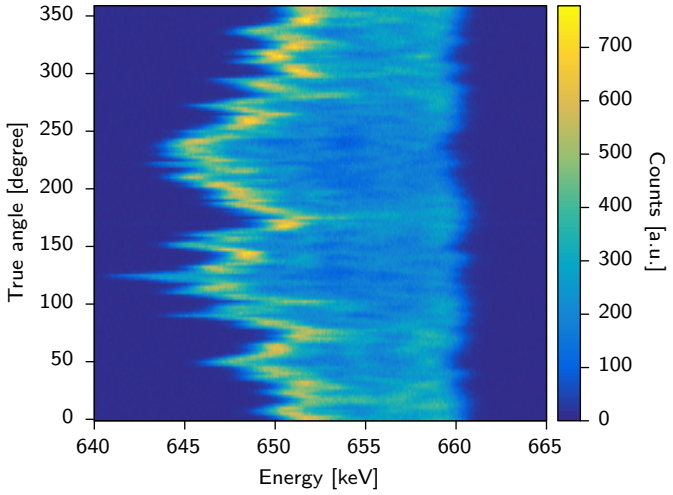

Figure 5: Single-site events around the 662 keV peak for ^{137}Cs measurements performed at discrete angles (1 mm collimation through the front face of the detector at a radius of 24 mm, with 2.5° increments). The y-axis represents the true angle of the measurement.

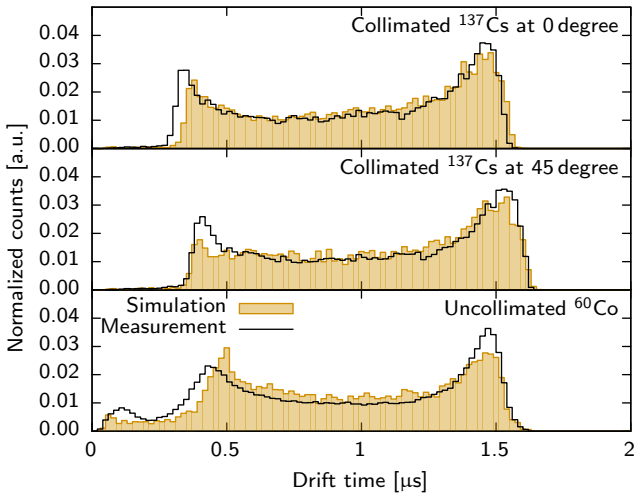

Figure 6: Simulated and measured drift-time distribution for three specific cases: Collimated ^{137}Cs single-site events in the 662 keV peak at 0° (along the ⟨100⟩ axis) and 45° (along the ⟨110⟩ axis) and uncollimated ^{60}Co single-site events in the 1332 keV peak.

proportional to the drift time. In practice, the detailed shape of the drift-time dependent energy correction factor was reconstructed from the centroid of the energy peak of 100 ns-wide drift-time regions and a linear interpolation between adjacent values.

However, it is also apparent in Fig. 4 that the peak distribution broadens with increasing drift time. Therefore, the amount of charge trapping must depend on additional parameters. This can be understood by returning to the idea of charge carriers drifting along a common path, as outlined in Sec. 2.4. Correcting the peak position according to the drift time effectively corrects charge trapping encountered along a single common path. As a result of the detector geometry, the path is common only for charge carriers that drift at the same azimuthal angle with respect to the center of the detector. However, variations in trapping are expected between angles. Fig. 5 displays the peak distribution as a function of the true angle and shows that charge trapping strongly depends on the azimuth. Thus, a drift time dependent energy correction must be determined for each angle separately and the events energy corrected according to both the azimuth and the drift time of that event. This is done by measuring the energy correction factor for each of the collimated ^{137}Cs measurement performed at different angles. The energy is then multiplied with the correction factor from the measurement that is closest to the events reconstructed azimuthal angle. The energy correction factors varies with angle and drift time and is between 0 and 5% of the total energy.

3. Drift time and azimuthal reconstruction results

Based on the methods described above, we report in this section the achieved performance of the segmented ICPC detector in terms of drift time extraction and azimuthal angle reconstruction. Comparisons with simulation are also presented.

3.1. Drift-time distribution

In order to define a simulated event's drift time, it is necessary to calculate the pulse shape. Such a procedure comes with uncertainties. In particular, the distribution of impurities throughout the detector is only accessible with limited precision. A linear longitudinal impurity gradient (from $0.64 \times 10^{10}\,\mathrm{cm}^{-3}$ at the front face's center to $1.60 \times 10^{10}\,\mathrm{cm}^{-3}$ at the rear face's center) was used. Furthermore, a linear radial gradient of $0.10 \times 10^{10}\,\mathrm{cm}^{-4}$ (increasing with increasing radius) was introduced. The adopted gradients are close to the impurity concentrations measured by the manufacturer (see Sec. 2.1), but not in perfect agreement. However, they provide the best reproduction of the observed measurements.

The simulated drift time distribution together with the respective measurements are presented in Fig. 6. Overall, for all three situations (collimated ^{137}Cs at two different azimuthal angles and uncollimated ^{60}Co) the simulations shows all features observed in data. Notably, the two bumps around 0.4 µs and 1.5 µs are well described. In the rear of the detector the drift-time isochrones curve towards the rear surface (see Fig. 3), thus the drift-time bins in that region correspond to events that occurred within a larger volume compared to other regions, explaining the first bump. The second bump is caused by γ-rays being more likely to interact close to the surface instead of penetrating far into the detector's interior. The deviations between measurements and simulations, particularly at short drift-times most likely originate from an incomplete description of the impurity concentration, particular in the radial dimension.

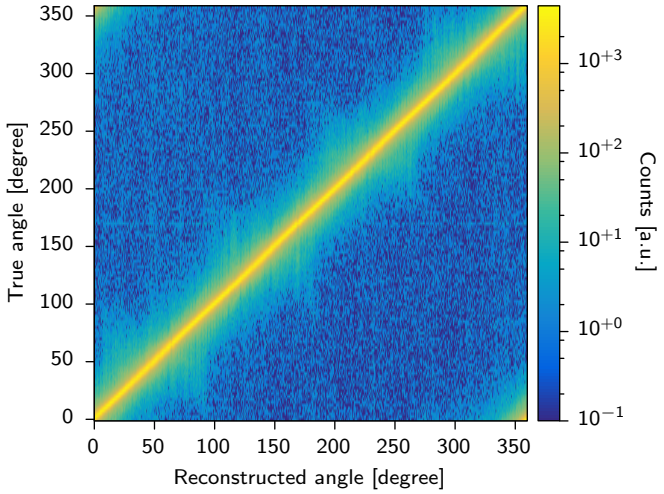

Figure 7: Reconstructed azimuthal angle (derived with the algorithm outlined in Sec. 2.5) displayed against the true angle for single-site events in the 662 keV peak from ^{137}Cs.

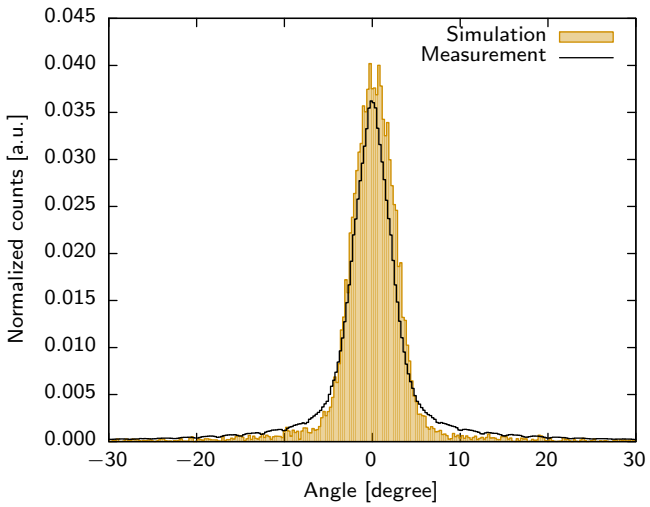

Figure 8: Deviation of the reconstructed angle from the true angle for single-site events in the 662 keV peak (black) and the actual angular position of simulated single-site events (orange).

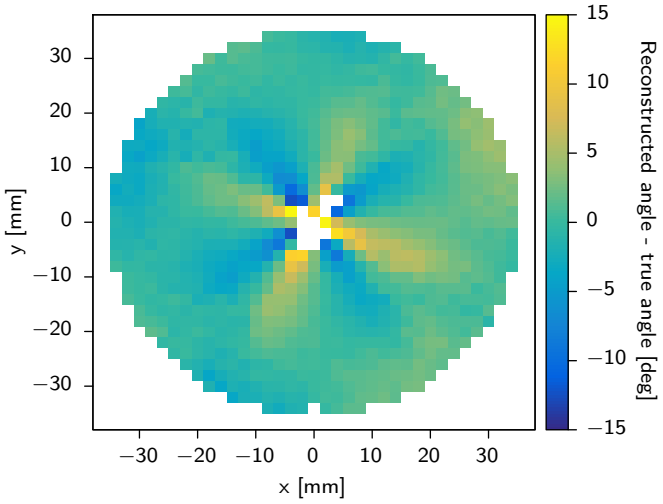

Figure 9: Difference between reconstructed angle and true angle of a collimated ^{241}Am surface scan measurement.

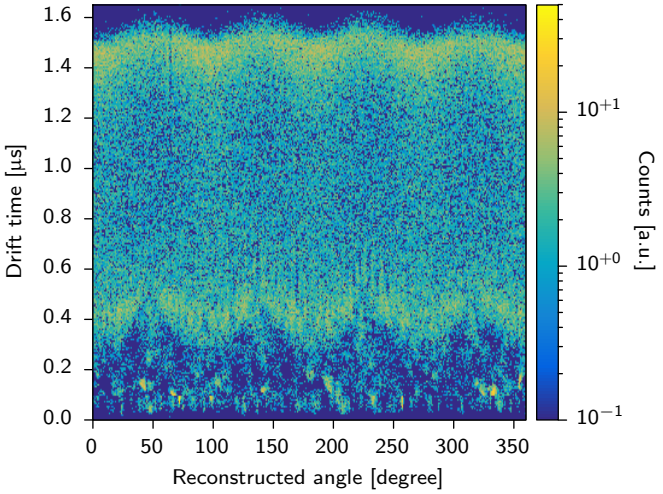

Figure 10: Distribution in the reconstructed angle vs drift-time plane for single-site events in the 1332 keV peak of an uncollimated ^{60}Co measurement.

3.2. Verification of azimuth reconstruction

There are many ways of analyzing the performance of the algorithm outlined in Sec. 2.5. One relatively straightforward method is to use the collimated ^{137}Cs source measurement used to construct the azimuthal basis. These data were taken at well known angles and provide a good initial test for the algorithm's performance. The results are summarized in Fig. 7 – the reconstructed and true angles are in overall good agreement. The difference between the true angle and the reconstructed angle effectively represents the average distribution of events around the location of the collimated source, as shown in Fig. 8. The measured distribution has strong tails, but the FWHM is $4.95° \pm 0.02°$, below the value of $5.77° \pm 0.11°$ observed for simulated single-site interactions. This suggests that the resolution is dominated by the size of the collimator and not the precision of the reconstruction method.

A more stringent test of the azimuthal reconstruction comes from ^{241}Am surface scans. Measurements with a collimated ^{241}Am source were taken on a regular 2 mm grid across the front surface of the detector. For each measurement the centroid of the distribution of the reconstructed angle can be compared to the actual location of the collimator. The difference between the average reconstructed angle and the true angle is displayed in Fig. 9. The discrepancy of up to 15° can be explained by the anisotropic drift velocity along crystal axes in germanium[12].

In this detector the ⟨100⟩ and ⟨110⟩ crystal axes lie in the x-y plane and are rotated by 45° with respect to each other (the azimuthal angle defined as 0° is roughly aligned with the ⟨100⟩ crystal axis). Before electrons reach the

common path, they drift predominantly in a radial direction. If the drift direction is not aligned with either of the two crystal axes, the anisotropic nature of the drift velocity causes an additional drift in the azimuthal dimension. The magnitude of the azimuthal drift is determined by the duration of the radial drift and thus by the radius at which the charges originate. However, the segments on the rear surface of the detectors are insensitive to this early charge motion. Once the electrons reach the common path, they drift towards the rear of the detector and start inducing image charges on the rear-surface segments. These signals are used for the azimuthal reconstruction and indicate at what angle, with respect to the constructed basis, the charges drift past the segments, but not at which angle they actually originate. Charges created at a radius that differs from the one at which the basis was calculated accordingly appear to be shifted with respect to this measurement. However, the reconstructed angle is the same for all charges that follow a specific common path and is a good parameter to study and correct variations in the average amount of trapping. The arising azimuthal shift can be corrected with a proper reconstruction of the radial position, outside the scope of this paper.

A further test of azimuthal reconstruction comes from an uncollimated ^{60}Co measurement, which should produce relatively evenly distributed events throughout the detector volume. Fig. 10 shows such a measurement, demonstrating that the angles are rather homogeneously reconstructed throughout the detector. Some clustering appears only at drift times below 300 ns. These events originate in a region relatively close to the 8 segments at the rear of the detector. The pulse shapes measured on these segments for such close interaction points are dominated by the contribution from holes drifting outwards, resulting in dissimilar pulse shapes. It is thus not surprising that the azimuth reconstruction method used is not precise in assessing the azimuth of these events. However, these events occur close to the point contact and are only weakly affected by charge trapping. An error in angular correction in that region is therefore not detrimental to the overall corrected energy. The sinusoidal features in Fig. 10, observed as a function of angle, are caused by the anisotropic drift velocity and the effect is consistent with the observed four-fold symmetry in the crystal.

4. Energy resolution results

The primary goal of this work was to investigate our capability to correct the energy observed in the ICPC detector for the effects of charge trapping associated with long charge drift times. Fig. 11 demonstrates the effects of the drift-time and azimuthal dependent corrections. As expected, without any correction the peak shape (orange line) is strongly distorted and shows multiple maxima. Such a peak is clearly not acceptable for γ-ray spectroscopy. The shape is considerably improved even with a correction for the drift-time dependence only (blue line). However,

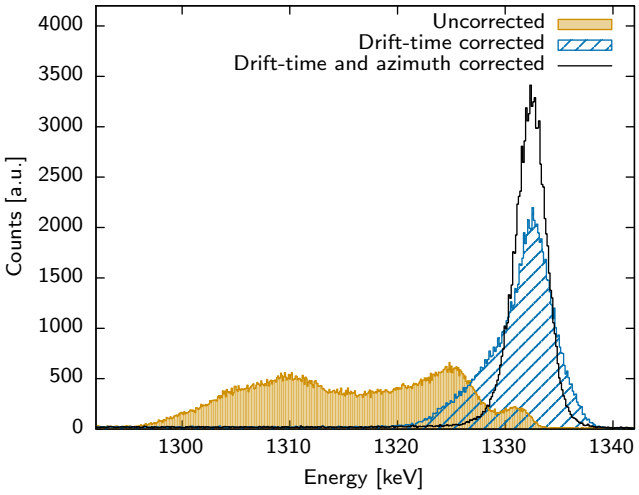

Figure 11: Shape of the 1332 keV peak of ^{60}Co (only single-site like event) with and without a correction of the energy.

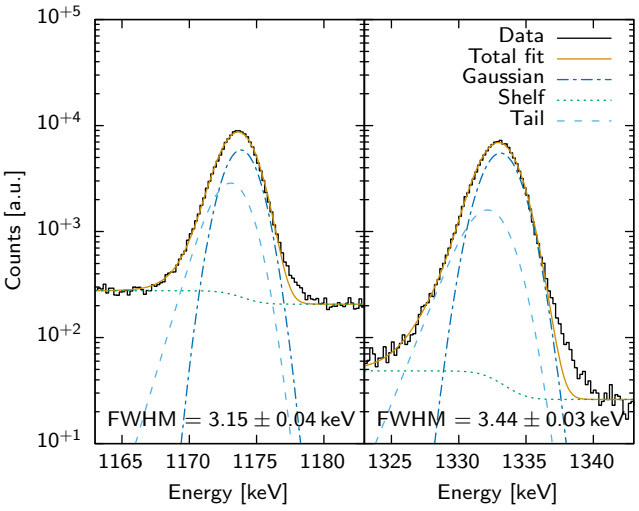

Figure 12: Fit to the 1173 keV and 1332 keV peak in ^{60}Co (only single-site like events). The fit function terms are defined in Ref. [13].

there remains a prominent low energy tail, which originates from large variations at long drift times. By including a correction for the azimuthal variations the peak is finally returned to a good Gaussian shape (black line). When both corrections are applied together the 1332 keV peak of ^{60}Co (see Fig. 12) has a FWHM of 3.44±0.03 keV (for the subset of events surviving the A/E cut). Fig. 13 and 14 show that the two corrections indeed remove most of the drift-time and azimuthal dependence. The centroid of the peak in both figures is found at a constant location and the width of the peak varies only slightly as a function of the drift time and the azimuth.

5. Discussion

By considering only single-site events with a short drift time (less than 300 ns) and using a simple drift-time cor-

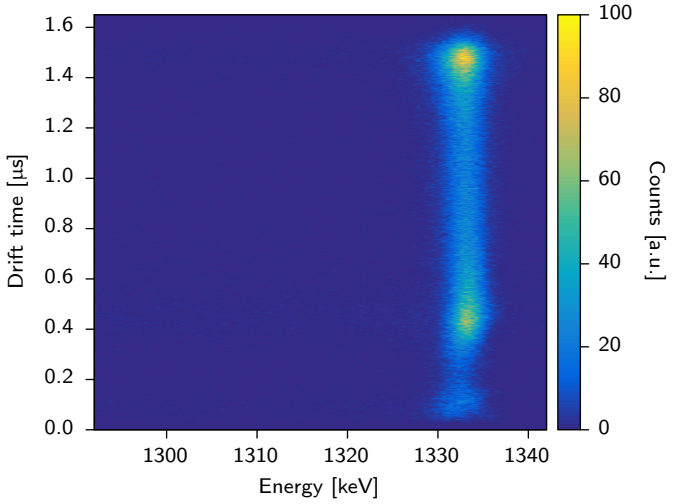

Figure 13: Drift-time dependence of single-site events in the region around the 1332 keV peak, with energy correction (see text).

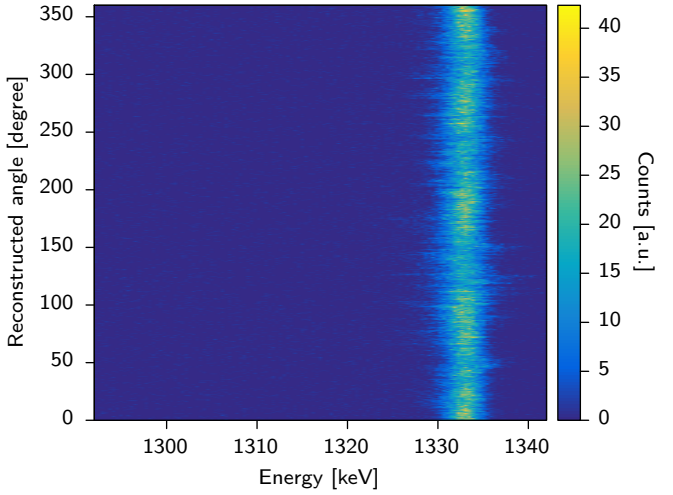

Figure 14: Angular dependence of single-site events in the region around the 1332 keV peak, with energy correction (see text).

rection without taking into account the azimuthal angle, the ICPC detector's resolution improves to 2.34 ± 0.05 keV at 1332 keV. This value is close to the resolution of 2.2 keV reported in Ref. [3] and shows that the detector performs close to other technologies within a limited volume. It also implies, that the overall resolution is still dominated by charge trapping effects and not by electronic noise or statistical effects in the number of created charge carriers. Hence, a better description of trapping effect could, at least in theory, improve the resolution to a value in that range.

It has been shown that there are regions where the described correction fails. In particular, the algorithm to extract the correct azimuthal angle is not robust for short drift times. However, charge trapping effects are inherently small at these drift times and the overall resolution is not strongly affected by these events. Instead, it is dominated by the dispersion of events observed at long drift times, an effect which has been largely corrected for with the azimuthal correction.

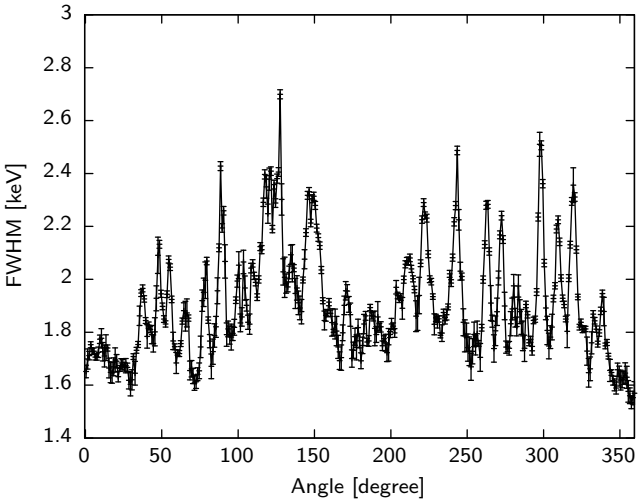

Figure 15: Angular dependence of the FWHM value of the 662 keV peak (single-site events only). Each data point represents a 1° slice.

Indeed, the ^{137}Cs data set measured at a constant radius can be subdivided into more refined angular slices. For each slice an individual drift-time dependent energy correction can be extracted. The width of the energy peak at 662 keV of individually corrected 1° slices is represented in Fig.15. It shows that variations in the width of the corrected peak appear over an angular scale larger than those represented by the respective data slices. An energy correction based on the 1° data division overall improves the resolution only by roughly 0.1 keV (single-site events in the 1332 keV peak). Thus, these deviations do not originate from an insufficient description of the angular dependence of charge trapping and the resolution cannot be considerably improved by a method that is only based on the azimuthal angle and the drift time of events. However, there are other variables, such as the radius at which an event occurs, that could provide a more complete description of trapping effects. The effect of radial variation has not yet been properly explored and should be addressed in a later publication, once a more complete position reconstruction is achieved.

It is also important to realize that the discussion so far has been limited to single-site like events, based on an A/E cut which corresponds to $\sim 13\%$ of all events at 1332 keV. If the above described algorithm is applied blindly to all events measured from an uncollimated ^{60}Co source, the peak resolution is degraded to 4.05 ± 0.01 keV. Thus, there is currently a trade off between detection efficiency (regulated with the A/E cut) and energy resolution. With a proper correction for the individual interactions, this effect should disappear and a similar energy resolution to the single-site event case is expected.

6. Conclusion

The paradigm to build detectors so that charge carriers are rapidly collected at the nearest electrode has governed n-type germanium detector technologies since their inception. However, it has been shown, that by intentionally abandoning this principle, new measurable quantities, such as the drift time and the normalized pulse height (A/E), that contain substantial information about the number and position of interactions, are accessible. Although the energy resolution in such a detector is drastically deteriorated as a result of charge trapping, we have shown that it can be restored for single-site events by applying a correction based on the information contained in the signals measured on the segments and the point contact.

The additional information available in the n-type segmented inverted coaxial point-contact detector certainly should simplify the reconstruction of interaction positions and potentially improve the position resolution compared to segmented coaxial detectors. In contrast, the energy resolution, although greatly improved, cannot yet compete with these detectors. However, while energy resolution is vital for γ-ray tracking and imaging arrays, in some applications (for example fast beam reactions) a good reconstruction of the position of individual interactions may be of comparable or even greater importance. The n-type segmented inverted coaxial point-contact detector, with the level of characterization completed to date, is a promising technology with a reasonable compromise between simple interaction position reconstruction and a good energy resolution.

Acknowledgment

This work is supported by LBNL-LDRD funding under LDRD NS16-128 and by the U.S. Department of Energy, Office of Science, Office of Nuclear Physics, under Contract No. DE-AC02-05CH11231 (LBNL) and Contract No. DE-AC05-00OR22725 (ORNL).

References

[1] R. J. Cooper, et al., Nucl. Inst. Methods Phys. Res. A 665 (2011) 25–32. doi:10.1016/j.nima.2011.10.008.
[2] P. N. Luke, et al., IEEE Trans. Nucl. Sci. 36 (1989) 926–930. doi:10.1109/23.34577.
[3] S. Paschalis, et al., Nucl. Inst. Methods Phys. Res. A 709 (2013) 44–55. doi:10.1016/j.nima.2013.01.009.
[4] J. D. Kephart, et al., J. Radioanal. Nucl. Chem. 282 (2009) 897. doi:10.1007/s10967-009-0216-2.
[5] R. Martin, et al., Nucl. Inst. Methods Phys. Res. A 678 (2012) 98–104. doi:10.1016/j.nima.2012.02.047.
[6] B. Bruyneel, et al., Eur. Phys. J. A 49 (2013) 61. doi:10.1140/epja/i2013-13061-4.
[7] Canberra Lingolsheim, 1, Chemin de la Roseraie, 67834 Tanneries Cedex, France, 2012.
[8] S. Agostinelli, et al., Nucl. Inst. Methods Phys. Res. A 506 (2003) 250–303. doi:10.1016/S0168-9002(03)01368-8.
[9] D. C. Radford, Siggen/Fieldgen, 2004. URL: http://radware.phy.ornl.gov/gretina/.
[10] D. Budjáš, et al., J. Instrum. 4 (2009) P10007. doi:10.1088/1748-0221/4/10/P10007.
[11] S. Sze, K. K. Ng, Physics of Semiconductor Devices, 2006.
[12] L. Mihailescu, et al., Nucl. Inst. Methods Phys. Res. A 447 (2000) 350–360. doi:10.1016/S0168-9002(99)01286-3.
[13] M. Salathe, T. Kihm, Nucl. Inst. Methods Phys. Res. A 808 (2016) 150–155. doi:10.1016/j.nima.2015.11.051.